

Neural circular RNAs are derived from synaptic genes and regulated by development and plasticity

Xintian You^{1,3}, Irena Vlatkovic^{2,3}, Ana Babic^{1,3}, Tristan Will^{2,3}, Irina Epstein^{2,3}, Georgi Tushev^{2,3}, Güneş Akbalik^{2,3}, Mantian Wang², Caspar Glock², Claudia Quedenau¹, Xi Wang¹, Jingyi Hou¹, Hongyu Liu¹, Wei Sun¹, Sivakumar Sambandan², Tao Chen¹, Erin M Schuman^{2,4} & Wei Chen^{1,4}

Circular RNAs (circRNAs) have re-emerged as an interesting RNA species. Using deep RNA profiling in different mouse tissues, we observed that circRNAs were substantially enriched in brain and a disproportionate fraction of them were derived from host genes that encode synaptic proteins. Moreover, on the basis of separate profiling of the RNAs localized in neuronal cell bodies and neuropil, circRNAs were, on average, more enriched in the neuropil than their host gene mRNA isoforms. Using high-resolution *in situ* hybridization, we visualized circRNA punctae in the dendrites of neurons. Consistent with the idea that circRNAs might regulate synaptic function during development, many circRNAs changed their abundance abruptly at a time corresponding to synaptogenesis. In addition, following a homeostatic downscaling of neuronal activity many circRNAs exhibited substantial up- or downregulation. Together, our data indicate that brain circRNAs are positioned to respond to and regulate synaptic function.

Cellular RNAs can exist in both linear and circular forms. Whereas a linear RNA possesses distinct 5' and 3' termini reflecting the start and end sites of transcription, the latter is formed by the covalent joining the 5' end of one exon with the 3' end of another, so-called head-to-tail splicing, resulting in a circular transcript. Recently, the deep sequencing of ribosomal RNA (rRNA)-depleted RNA, combined with computational tools, has led to the identification of thousands of new circRNAs in organisms ranging from Archaea to human^{1–3}. For many years, no clear function was attributed to any of the circRNAs, but it was recently demonstrated that two previously identified circRNAs can serve as miRNA 'sponges'^{4,5}, sequestering miRNAs and preventing their interactions with target mRNAs. Although this observation offers one model for circRNA function, circRNAs represent a heterogeneous group of transcripts that likely also affect cellular function via as yet undiscovered and diverse mechanisms. In addition to miRNA regulation, it has been proposed, for example, that circRNAs could sequester RNA-binding proteins (RBPs) and thereby regulate the intracellular transport of associated RBPs or RNAs^{6,7}.

The regulation of cellular function and protein translation by RNA-mediated mechanisms is exploited in many polarized cells to functionalize cellular compartments. This is particularly evident in neurons, where the complex morphology and distal location of synapses mandate a high degree of local regulation⁸. Indeed, localized protein synthesis has been observed in both dendrites and growing axons, owing to the localization of translational machinery and over 2,000 mRNAs in each compartment^{9,10}. In recent years, other types of RNA species and RNA-based regulation have been identified in neurons, including miRNAs

and lncRNAs^{11,12}. We examined the expression pattern of circRNAs and found that circRNAs were enriched in the brain relative to other tissues. We discovered that a disproportionate fraction of circRNAs were derived from host genes that code for synaptic proteins. Using PacBio sequencing of reverse transcription PCR (RT-PCR) products for a subset of circRNA candidates, we identified rolling circle sequences indicating, to the best of our knowledge for the first time, a true circular structure. At the same time, we determined the full-length sequences of these circRNAs and demonstrated the alternative usage of internal exons from the circRNAs with the same head-to-tail junctions. Furthermore, based on the separate profiling of the RNAs localized in neuronal cell bodies and synaptic processes (axons and dendrites), we found that, on average, circRNAs were more enriched in synaptic processes than their linear isoforms. Using high-resolution *in situ* hybridization, we visualized a subset of circRNAs directly in the dendrites of neurons. Finally, we found that the abundance of several circRNAs changed at developmental stages that correspond to synapse formation and following homeostatic plasticity.

RESULTS

CircRNAs are enriched in brain

To systematically determine the tissue-specific expression pattern of mammalian circRNAs, we deep-sequenced rRNA-depleted total RNA samples from different mouse tissues, including brain, heart, liver, lung and testis (Fig. 1a). From two biological replicate experiments in each tissue, we obtained a minimum of 16×10^6 reads and a maximum of 21×10^6 reads, with mappable reads ranging from 88.7 to 96.1%

¹Berlin Institute for Medical Systems Biology, Max-Delbrueck-Center for Molecular Medicine, Berlin, Germany. ²Max Planck Institute for Brain Research, Department of Synaptic Plasticity, Frankfurt, Germany. ³These authors contributed equally to this work. ⁴These authors jointly directed this work. Correspondence should be addressed to E.M.S. (erin.schuman@brain.mpg.de) or W.C. (wei.chen@mdc-berlin.de).

Received 30 September 2014; accepted 10 February 2015; published online 25 February 2015; doi:10.1038/nn.3975

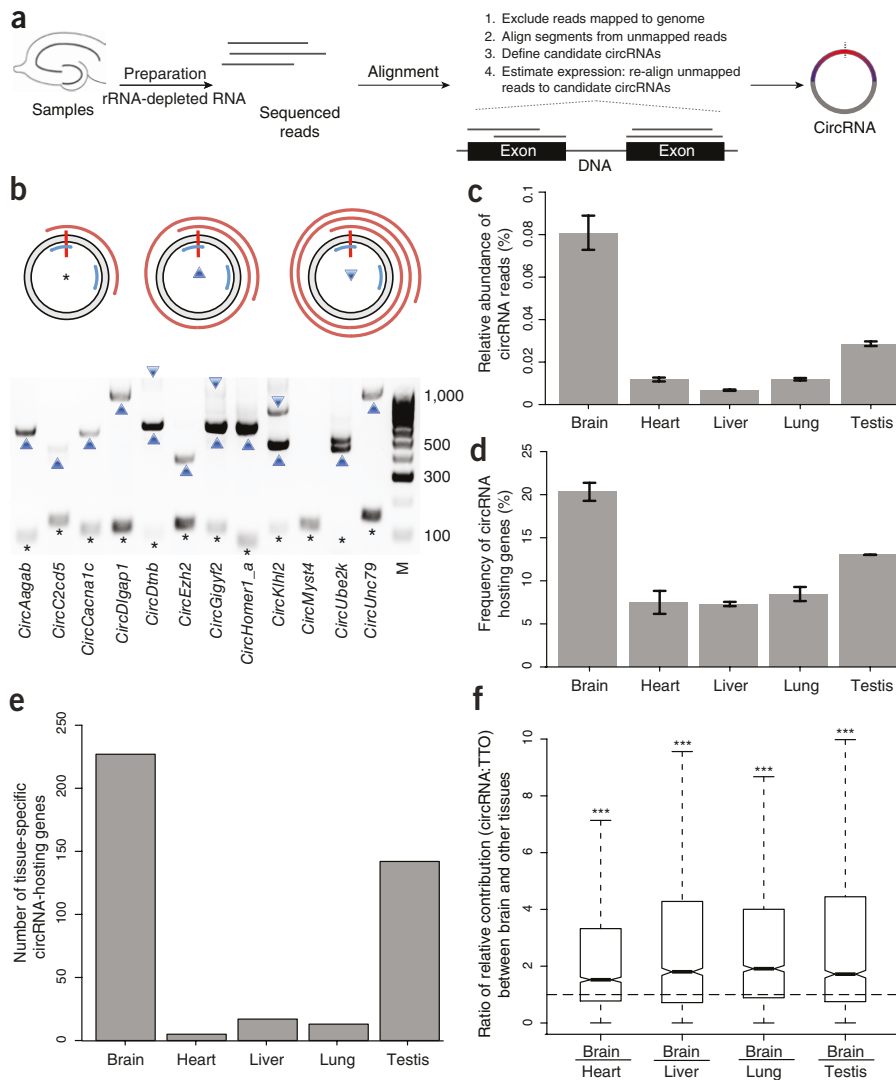


Figure 1 Profiling of circRNAs across tissues reveals enrichment in brain. **(a)** Experiment and analysis pipeline. **(b)** The rolling circle cDNA products from circRNAs. The gray ring represents a circRNA and the red vertical bar marks the head-to-tail junction. Two blue arcs mark the PCR primers. The red spirals on the outside represent PCR products that were deep sequenced by PacBio technology. The asterisk, upward triangle and downward triangle symbols on the gel image denote the 0-cycle, 1-cycle and 2-cycle RT products identified by PacBio sequencing, respectively. 11 of 12 circRNAs tested generated rolling circle products (the exception was *circMyst4*). **(c)** The percentage of circular junction reads (from Ensembl genes) from all the reads mapped on the genome is shown for different tissues, with the highest value (0.075–0.087%) in brain, followed by testis (0.028–0.029%). **(d)** The percentage of genes that produced circRNAs from all the expressed genes is shown across different tissues, with the highest value (20–21%) in brain, followed by testis (13%). **(e)** The number of circRNA host genes that are exclusively expressed in one tissue is shown across different tissues, with the highest value in brain. **(f)** The relative contribution of circRNA to the TTO of the same gene locus, that is, the ratio between the abundance of each circRNA and the TTO of the hosting gene loci (measured in TPM), was significantly higher in brain than in all other tissues. The ratios of the relative contribution between brain and other four tissues were significantly larger than 1 (two-sided one-sample *t*-test, ****P* < 2.2 × 10⁻¹⁶). Tissues in c–f were obtained from two animals. Error bars represent s.d. (c,d,f).

products (Fig. 1b), which could not be detected in the cDNAs from any linear forms. This serves as direct evidence for the circular nature of the circRNA structure and, to the best of our knowledge, is the first time that

depending on the tissue (Table 1). Reads that map directly to reference genome sequences or canonical exon-exon junctions can be derived from either linear RNAs or circRNAs and were therefore used to estimate the expression of the total transcriptional output (TTO) of the corresponding gene loci. To specifically identify circRNAs, we used the remaining reads that spanned the 5' and 3' splicing sites of exon(s) of individual genes, but in reverse order (head-to-tail junction reads; Fig. 1a and Online Methods). From the five tissues, we detected a total of 13,011 unique circRNAs.

We validated the authenticity of identified circRNAs by three independent methods. First, as circRNAs usually do not possess a poly(A) tail, their representation should be depleted in a poly(A)-enriched sequencing library. Compared with rRNA-depleted total RNA sequencing, poly(A) RNA sequencing produced a much lower number of sequencing reads derived from our circRNA population (Supplementary Fig. 1a). Second, compared with linear RNAs, circRNAs are endowed with a strong resistance to the exonuclease RNase R. We therefore quantified the RNase R resistance of 20 candidate circRNAs, and all of them exhibited greater than five-fold higher stability than the linear transcripts following RNase R treatment (Supplementary Fig. 1b). Third, we deep sequenced the cDNA products derived from 12 candidate circRNAs. For 11 of them, we observed the cDNA reads corresponding to the rolling circle RT

the full sequences of the circRNAs have been identified. Notably, for two circRNAs (*circDtnb* and *circEzh2*), in addition to the 'canonical' forms that encompass all of the annotated exons between the two involved in the back-splicing, we also observed circular isoforms that consisted of the same junction sequences, but with one internal exon skipped (*circDtnb*) or one unannotated exon inserted (*circEzh2*) (Supplementary Tables 1 and 2).

Although circRNAs were observed in all of the tissues that we examined, their abundance was clearly highest in brain (Fig. 1c and Supplementary Fig. 1c), where 20% of the protein-coding genes produced circRNAs (Fig. 1d and Table 1). Two factors contributed to the higher abundance of circRNAs in brain. First, many host genes that produce circRNAs were expressed exclusively in brain (Fig. 1e and Supplementary Fig. 1c). Second, on average, when a host gene was expressed in brain as well as other tissue(s), the relative contribution of circRNAs (defined as the ratio of TPM between a circRNA and the TTO of its host gene locus, where TPM is a measure of relative transcript abundance defined as transcripts per million) was significantly higher in brain than in all other tissues (*P* < 2.2 × 10⁻¹⁶; Fig. 1f and Supplementary Fig. 1c). We also reanalyzed published RNA-seq data sets from different tissues of rat¹³ and observed a similar enrichment of circRNAs in brain (Supplementary Fig. 1d). Together, our data and analyses demonstrate that circRNAs, as a group, are enriched in brain.

Table 1 Summary of RNA-seq results for five different mouse tissues

	Brain		Heart		Liver		Lung		Testis	
	Replicate 1	Replicate 2	Replicate 1	Replicate 2	Replicate 1	Replicate 2	Replicate 1	Replicate 2	Replicate 1	Replicate 2
Total number of reads	19,794,174	19,164,999	16,507,635	19,876,852	21,001,677	19,056,514	20,390,058	18,406,517	19,940,919	20,222,389
Number of reads mapped on genome	18,765,595	18,283,420	14,636,897	19,049,052	20,195,791	18,322,339	19,595,737	17,282,775	18,802,286	19,198,630
Number of reads mapped on intronic regions	6,884,089	6,971,714	3,028,058	4,629,968	4,184,807	3,926,699	9,071,821	7,834,607	4,611,925	5,042,735
Number of reads mapped on intergenic regions	2,125,517	1,862,307	2,353,147	1,381,043	1,196,394	1,141,757	1,854,519	2,078,503	3,909,966	3,954,450
Number of reads mapped on protein coding genes	8,290,663	8,085,776	7,775,596	11,156,730	13,316,937	12,017,101	7,516,840	6,480,473	9,450,865	9,429,187
Number of protein coding genes expressed (TPM > 5)	11,781	11,763	10,044	9,824	8,261	8,248	11,987	11,882	10,665	10,684
Number of circular junction reads	16,573	14,068	1,646	2,393	1,442	1,231	2,453	2,024	5,606	6,053
Number of circRNA species	6,186	5,664	989	1,315	912	816	1,556	1,320	2,943	3,093
Number of circRNA-hosting protein coding genes	2,569	2,386	707	869	676	637	1,116	955	1,480	1,482

circRNAs: synaptic gene origin and dendritic localization

Is the likelihood that a given linear transcript will be spliced to produce a circRNA related to the host gene function? To address this, we conducted a Gene Ontology analysis of the genes that give rise to brain-expressed circRNAs (Online Methods). Notably, several functional groups related to synaptic function, such as synapse, synapse part, presynaptic active zone, presynaptic membrane and postsynaptic density, were significantly enriched ($P < 0.001$, Fig. 2a). This enrichment was present regardless of the expression level of the host genes (Supplementary Fig. 2a).

Given the enrichment of host genes with synapse-related functions, we next examined whether the circRNAs are enriched in synaptic tissue. To address this, we prepared synaptosomes, a biochemically purified preparation that is enriched in synapses^{14,15}, or microdissected the synaptic neuropil from the hippocampus, a brain structure that exhibits robust synaptic plasticity and is important for learning and memory¹⁶. We then compared the abundance of circRNAs in these compartments (synaptosomes or neuropil) to that observed in a whole hippocampal homogenate or a microdissected layer comprising primarily hippocampal neuronal somata. We found that most circRNAs were indeed enriched in either or both of the two synaptic fractions examined (Fig. 2b and Supplementary Fig. 2b) and the overlap between the two synaptic fractions was statistically significant ($P < 2.2 \times 10^{-16}$, Fisher exact test; Supplementary Fig. 2d). The same pattern of results was observed when the tissue was obtained from rat (Supplementary Fig. 2c) and there was substantial overlap between the circRNAs identified in mouse and rat (Supplementary Fig. 2e).

To validate the enrichment of circRNAs in the biochemically or manually dissected synaptic compartments, we directly visualized the circRNAs in cultured hippocampal neurons using high-resolution *in situ* hybridization⁹ optimized for the detection of circRNAs (Online Methods and Supplementary Fig. 3a,b). Using an *in situ* probe set designed for the detection of *circHomer1_a*, a circRNA derived from the synaptic scaffolding molecule Homer1 transcript¹⁷, we detected *circHomer1_a* particles in the cell bodies and dendrites (visualized by an antibody to MAP2) of neurons (Fig. 2c). In contrast, use of an exon

control probe set (using a sequence from two exons that do not form a circRNA) resulted in a markedly reduced signal with only one or two particles evident in the vicinity of the cell bodies and nuclei (Fig. 2c and Supplementary Fig. 3b). Use of additional probes developed for the detection of circRNAs derived from synapse-related genes, including *circDscam*, *circKlhl2*, *circElavl3*, *circNlgn1*, *circGigyl2*, *circNbea* and *circRmst*, resulted in a similar pattern with abundant particles present in the cell body and distributed particles observed throughout the dendritic arbor (Fig. 2c and Supplementary Fig. 3e–j). In hippocampal slices, *in situ* hybridization using a *circHomer1_a* probe revealed substantial expression of this circRNA in both somata and neuropil layers of CA1 hippocampal region (Fig. 2d). In addition to the exon control, scrambled probe and no probe control experiments (Fig. 2c and Supplementary Fig. 3c,d), we validated the specificity of our circRNA *in situ* hybridization by comparing the signal intensity of *circRmst*, *circKlhl2* and *circGigyl2* in brain, liver and lung (Supplementary Figs. 3 and 4). Consistent with the RNA-seq data, the *in situ* hybridization data revealed only background levels of expression of *circRmst* and *circKlhl2* in liver and lung, whereas these circRNAs were clearly evident in hippocampal neurons. In contrast, *circGigyl2* was expressed in all examined tissues as expected from RNA-seq data (Supplementary Fig. 4). To test whether the circRNA localization can mimic that of its host transcript, we performed *in situ* hybridization of *circRims1* and its host mRNA *Rims1* in cultured hippocampal neurons. Although signals for the circRNA and mRNA were apparent in both cell body and dendrites, they clearly did not colocalize (Supplementary Fig. 5). Given the anticipated diversity of circRNA populations, however, one must be open to counterexamples of colocalization of circRNA and mRNA when more cases are examined.

Absence of miRNA and RBP binding or translation into protein

Recent studies of two individual circRNAs suggested that they function as miRNA sponges, sequestering miRNAs^{4,5}. Using a bioinformatics approach, we estimated the potential of the brain circRNA population to serve as miRNA sponges and concluded that, as a general class, the brain circRNAs do not exhibit a greater capacity to serve as miRNA

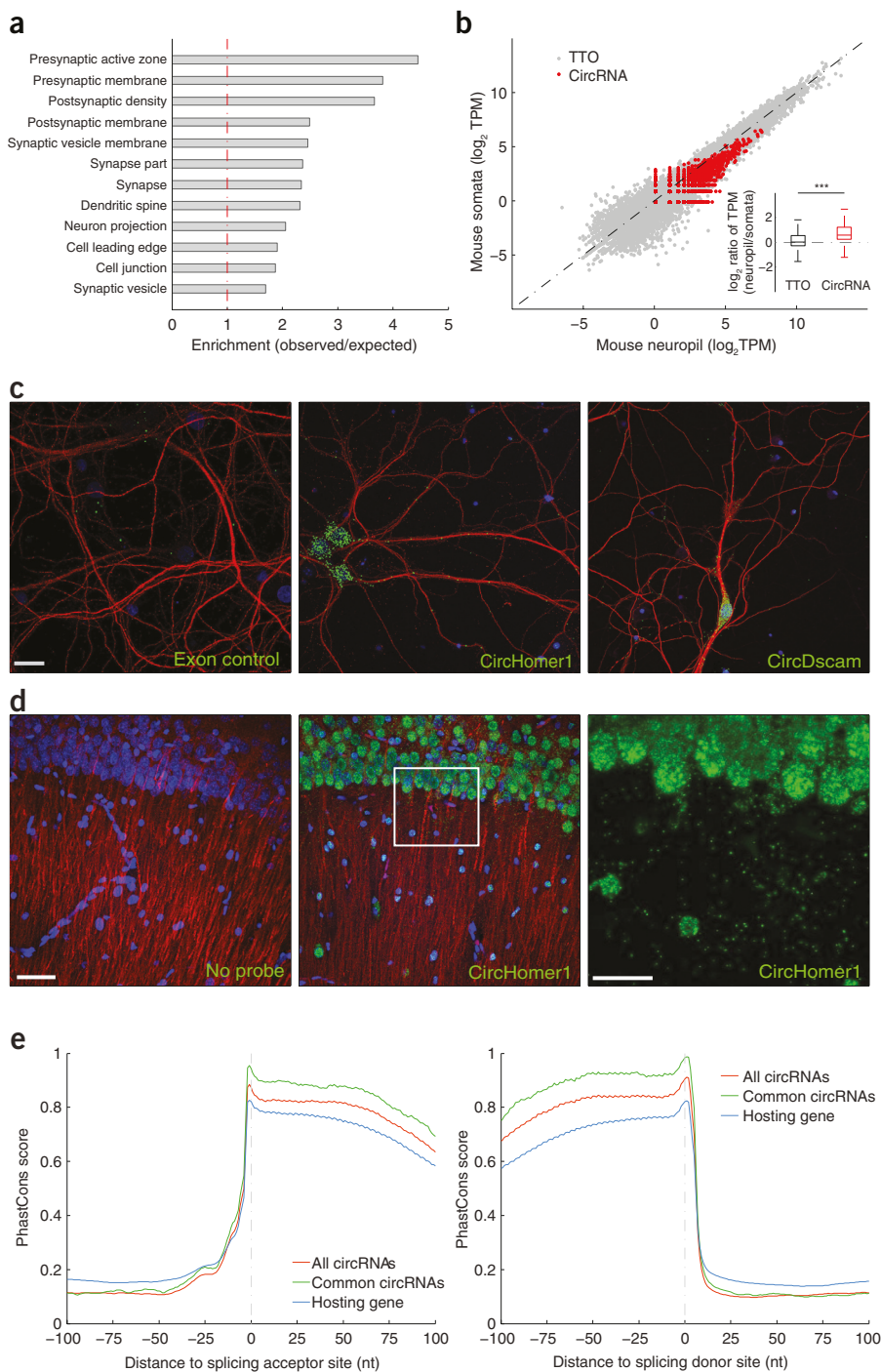


Figure 2 Brain expressed circRNAs are derived from genes coding for synaptic proteins and are enriched in synaptic tissues. **(a)** Gene Ontology enrichment analysis of the genes producing brain-expressed circRNAs. Functional groups related to synaptic function were overrepresented in the genes producing brain circRNAs. **(b)** The abundance of circRNA and TTO of protein-coding gene loci (measured in TPM) were compared between neuropil (x axis) and the somatic layer of the hippocampus (y axis) in mouse. Each red dot represents one circRNA, and each gray dot represents one protein-coding gene locus. Inset shows that the abundance of circRNAs, but not TTO, was significantly higher in the synaptosome and neuropil fractions (two-sided, unpaired Student's *t*-test, *** $P < 2.2 \times 10^{-16}$). **(c,d)** High-resolution *in situ* hybridization experiments in cultured hippocampal neurons **(c)** or hippocampal slices **(d)** using probe sets designed to detect the indicated circRNA (green). In each case, many circRNA-positive particles are apparent in the cell bodies (nuclei stained with DAPI, blue) as well as in the dendritic processes, as detected using an antibody to MAP2 (red). A control (exon) probe designed to detect non-contiguous regions of two exons that could not form head-to-tail junction (Online Methods) yielded just a few background particles. Scale bars represent 20 **(c)**, 50 **(d)** and 75 μ m **(d, right)**. For cells, one representative image from 3–43 images is shown, for slices, one image from four images is shown. **(e)** The exonic sequences around the splicing sites (left, splicing acceptor; right splicing donor) involved in the formation of mouse circRNA head-to-tail junctions (red) were more conserved than those from the same gene locus, but not involved (blue). y axis denotes the average PhastCons score. x axis marks the distance to the splicing site (negative and positive values means upstream and downstream, respectively). Notably, the exonic sequences around the circRNA junctions common in mouse and rat (green) were even more conserved, almost reaching the maximum PhastCons score.

sponges than linear mRNAs (Supplementary Fig. 6a), consistent with recent analyses from other groups¹⁸.

We also examined the possibility that brain circRNAs might function to bind or sequester RBPs. For this purpose, we predicted the binding sites of 38 RBPs based on their binding sequence motifs deposited in the database RBPDB (Online Methods). CircRNAs possess a lower RBP binding density, when compared to either the coding sequence or the 3' UTR of protein-coding genes (Supplementary Fig. 6b). This trend is consistently observed for circRNAs of different abundances (Supplementary Fig. 6b). Thus, these data indicate, based on nucleotide sequence alone, that circRNAs as a group are no more likely to bind to RBPs than linear mRNAs.

As a result of the well-known low detection sensitivity of MS-based shotgun proteomics approaches. Thus, we further studied the association of circRNAs with ribosomes. First, we performed ribosome profiling¹⁹ on rat brain. Similar to what was recently reported for circRNAs from a human cell line¹⁸, in our rat brain samples, we did not detect a single ribosome-protected fragment (RPF) that mapped to a circRNA head-to-tail junction and could therefore serve as evidence for circRNA translation. This negative finding could be a result of the short read length of RPFs and, more importantly, the ribosome might only associate with the sequences outside the junction. To circumvent this limitation, we performed polysome profiling on mouse brain. In contrast to mRNAs, circRNAs were enriched in the non-ribosomal RNA fraction

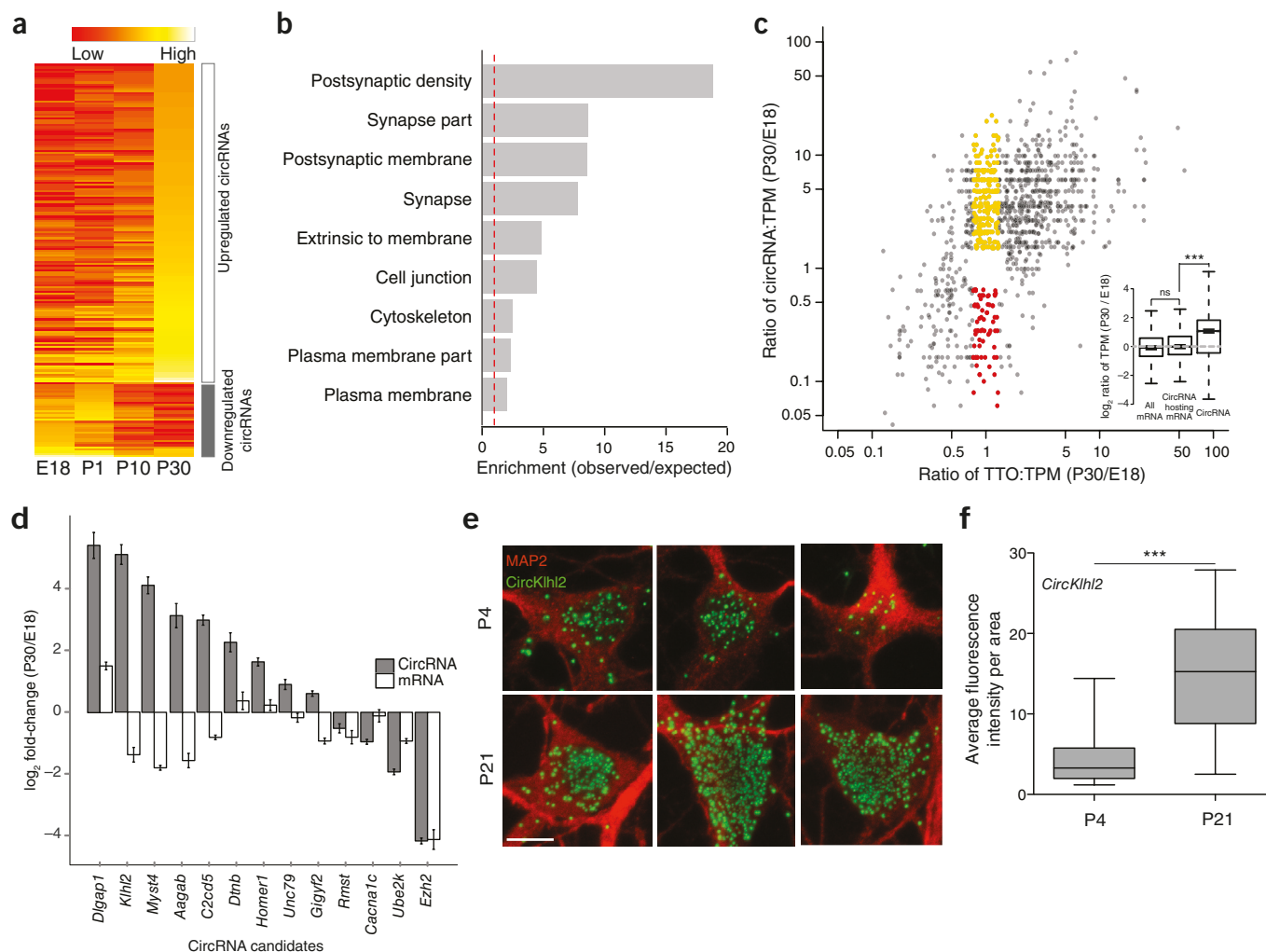


Figure 3 Regulated expression of brain circRNAs during development. **(a)** Heatmap of circRNA expression across four different developmental stages showing the regulation of several circRNA clusters between P0 and P10, the time at which synapses typically form. The abundance of circRNAs across four developmental stages is depicted on a scale from red (low) to yellow (high). A developmentally downregulated cluster consisting of 43 circRNAs exhibited an early peak expression at E18 or P1 and then declined over subsequent developmental time points. A developmentally upregulated cluster, consisting of 181 circRNAs, exhibited increasing expression that peaked at P10 or P30. **(b)** The significantly enriched GO terms ($P < 0.05$ in either cluster). The host genes with circRNAs that exhibited peak expression associated with the time of synapse formation were enriched for synaptic function whereas the other group (downregulated) did not exhibit significant enrichment of any GO terms. **(c)** Fold change of both circRNA abundance (y axis) and the TTO of their gene loci (x axis) between stages E18 and P30. Each dot represents one circRNA. Dots in red and yellow highlight circRNAs that changed significantly while the TTO of their host loci was not substantially altered. Inset shows that, although most circRNA-hosting genes did not change much in abundance compared to all genes (two-sided unpaired Student's t -test, ns indicates $P = 0.09709$), circRNAs were significantly upregulated (two-sided unpaired Student's t -test, *** $P < 2.2 \times 10^{-16}$). Six or seven mice were pooled in each of two replicates of E18. Three or four mice were pooled in each of two replicates of P30. **(d)** The expression change for both circRNA and mRNA was validated using quantitative PCR for 13 circRNAs, including *Homer1*, *Dlgap1*, *Rmst*, *Myst4* and *Ezh2*. Error bars represent s.d. **(e,f)** Validation of circRNA expression changed over developmental stages using high-resolution *in situ* hybridization for circKhlh2 (green) at two time points, 4 ($n = 26$) or 21 ($n = 24$) d in culture. *circKhlh2* expression was significantly upregulated between these developmental stages (two-sided unpaired Student's t test with Welch's correction, *** $P < 0.0001$). The outline of the neuronal somata was identified using an antibody to MAP2 (red). Scale bar represents 10 μ m.

and strongly depleted in the ribosome/polysome-bound fractions (Supplementary Fig. 6c,d). Together, these results demonstrate that circRNAs, as a group, are unlikely to be translated into peptides.

Conservation of circRNA para-junctional sequences

Given that functionally important elements are often evolutionary conserved, we examined the sequence conservation around the mouse circRNA junctions. Compared with splicing sites from the same hosting genes that are not involved in forming head-to-tail junctions, the exonic sequences around head-to-tail junctions were more conserved (Fig. 2e). Moreover, those sequences around common head-to-tail

junctions detected in both mouse and rat were even more conserved, almost reaching the maximum PhastCons score. The observation that exonic sequences around circRNA junctions are extremely conserved evolutionarily in vertebrates is a strong indicator of their potential functional relevance.

Expression of circRNAs in brain during development

To determine whether the expression of circRNAs is developmentally regulated in brain, we profiled the circRNA population in the hippocampus over several stages: embryonic (E18), early postnatal (P1), postnatal at the beginning of synapse formation (P10) and late postnatal

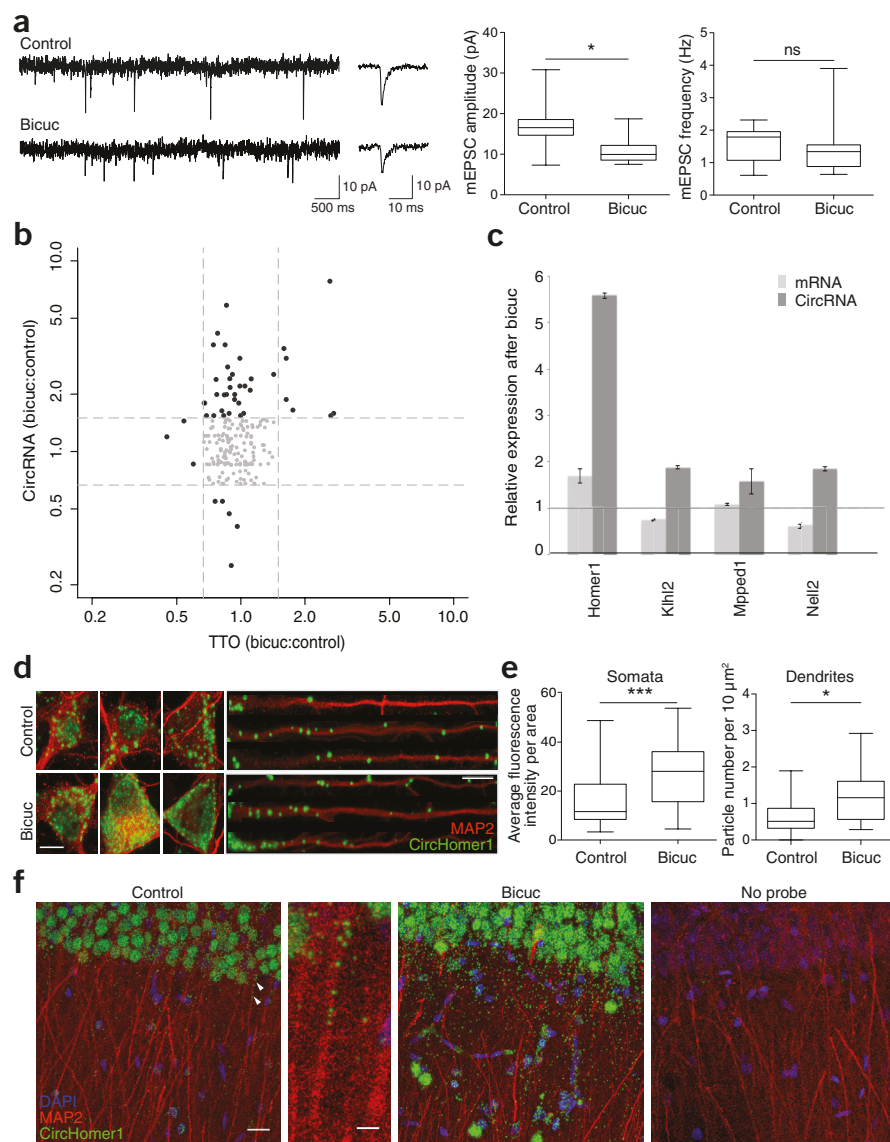


Figure 4 Regulation of circRNAs by homeostatic plasticity. **(a)** Electrophysiology traces of mEPSCs from control cultures and cultures treated with bicuculline for 12 h. Shown are representative recordings (left), the average mEPSC waveform and quantification of mEPSC amplitudes and frequency (right) ($n = 8$ cells each for control and bicuculline treatment, $*P < 0.0499$ for amplitude and $P < 0.3717$ for frequency). **(b)** Expression changes of circRNA (y axis) and TTO (x axis) after homeostatic plasticity. Each dot represents one circRNA. Gray dots represent circRNAs in which expression remained largely the same (less than 30% change) for both circRNA and TTO. **(c)** Quantitative PCR validation of expression change for both circRNAs and their cognate host mRNAs following plasticity (error bars represent s.d.). **(d)** Validation of circRNA expression changes following homeostatic plasticity using high-resolution *in situ* hybridization for *circHomer1_a* in control or bicuculline-treated neurons. Dendrites were identified using an antibody to MAP2. Scale bars represent 10 μm . **(e)** *circHomer1_a* expression was significantly upregulated in both the neuronal somata (n for control = 34, n for bicuculline = 43, $***P < 0.0005$) and dendrites (n for control = 12, n for bicuculline = 13, $*P < 0.0208$) following homeostatic plasticity. Primary hippocampal cell cultures were prepared from 10–20 animals. **(f)** *circHomer1_a* expression was significantly upregulated in hippocampal slices following homeostatic plasticity. From left to right, control slice, zoom of a region of the control slice (indicated by arrowheads) showing presence of several *circHomer1_a* in a continuous stretch of dendrites, bicuculline-treated slice and no probe control. Scale bars represent 20 μm (left) and 5 μm (right). Bicuculline-treatment resulted in a significant upregulation of *circHomer1* in both stratum pyramidale (somatic layer) and stratum radiatum (neuropil layer) ($n = 3$ slices each for control and bicuculline treatment, $P < 0.0005$ for somata and $P < 0.0011$ for neuropil).

hippocampus following the establishment of mature neural circuits (P30) (Supplementary Fig. 7). There was a clear shift in the circRNA expression pattern associated with the onset of synaptogenesis at P10 (Fig. 3a). Notably, the circRNAs that were consistently upregulated during hippocampal development were produced from the gene loci that also code for proteins enriched with synapse-related functions (Fig. 3b). In contrast, no enrichment of any functional categories could be observed for the gene loci showing the opposite (downregulated) circRNA dynamic expression pattern.

We next examined the relationship between the expression of a circRNA and its linear host comparing the earliest (E18) and latest (P30) developmental stages. We found that many circRNAs change their expression independent of their host transcripts during synaptogenesis (Fig. 3c). We validated 13 circRNA and mRNA pairs with different expression patterns using quantitative PCR (Fig. 3d). *Dlgap1*, whose protein product is a core component of postsynaptic density (PSD), showed a >20-fold increase in circRNA expression at P30 when compared with E18, whereas the mRNA expression increased by less than four fold. Genes such as *Myst4*, *Khlh2* and *Aagab* markedly increased their circRNA expression over the course of development, whereas their mRNA expression markedly decreased. In contrast, *Cacna1c* showed

substantial decreases in circRNA expression along developmental stages, whereas the mRNA remained unchanged. Using high-resolution *in situ* hybridization in cultured hippocampal neurons, we further validated the developmental regulation of *circKhlh2* that exhibited strong upregulation during development (Fig. 3e). Analysis of the average fluorescence intensity at an early and late developmental stage (neurons cultured beginning at P1, days *in vitro* = 4 or 21) revealed a significant enhancement of the *circKhlh2* expression levels ($P < 0.0001$; Fig. 3f). Taken together, our data from high-throughput sequencing, quantitative PCR and *in situ* hybridization indicate that the expression of circRNAs is developmentally regulated in neurons and that many circRNAs change their expression independent of their host linear transcripts.

Neuronal plasticity changes circRNA expression

If circRNAs regulate synaptic function, then their expression levels might be modulated by alterations in neuronal activity and plasticity. We induced homeostatic synaptic plasticity in cultured hippocampal neurons by manipulating neuronal activity using bicuculline, an antagonist to the GABA_A receptor. Treatment with bicuculline enhanced excitatory neuronal network activity, leading to a homeostatic decrease in the mini-excitatory postsynaptic current (mEPSC) amplitude, without a change in mEPSC frequency (Fig. 4a)²⁰. Following

induction of homeostatic plasticity, the circRNA population exhibited dynamic behavior: the expression of 37 circRNAs was enhanced (Fig. 4b), whereas that of 5 circRNAs was reduced. In contrast, most of their linear host transcripts showed no substantial change in expression level (Fig. 4b). We validated the plasticity-induced changes in four circRNA candidates using quantitative PCR (Fig. 4c). We also visualized directly the circRNA expression changes after homeostatic plasticity for additional candidates using *in situ* hybridization. *CircHomer1_a* was significantly upregulated in primary hippocampal neurons ($P < 0.0005$ for somata and $P < 0.0208$ for dendrites) (Fig. 4d,e) and hippocampal slices (Fig. 4f). Taken together, these data indicate that circRNA expression levels are regulated by neural plasticity, suggesting that they are important for regulating synaptic transmission and/or local translation.

DISCUSSION

Eukaryotic circRNAs are a class of low-abundance, but biochemically stable, cellular RNAs that possess neither a 5' nor a 3' end. The property of circularity has contributed to their relative anonymity (until recently), as most of the transcriptome-wide studies begin with the purification of a poly(A)+ RNA fraction. Similar to other recent studies^{2,5,18,21}, we sequenced and analyzed rRNA-depleted samples that allow one to analyze circRNAs and their linear host transcripts in a quantitative manner. Whereas circRNA identification relied on available genome annotation in previous studies^{2,5}, we set up a computational pipeline that does not rely on exon annotations or assume canonical splice sites, and can therefore identify circRNAs derived from previously unannotated exons and transcripts. This allowed us to identify the circRNAs in rat, which, to date, has a relatively incomplete transcriptome annotation.

We validated our findings with several independent approaches. Notably, using PacBio deep sequencing of the cDNA products derived from candidate circRNAs, we observed reads that corresponded to the rolling circle RT products, which serves as direct evidence for the circular nature of the RNA and provides the full-length sequences of the circRNAs. On the basis of the sequences, we identified, to the best of our knowledge for the first time, circRNA isoforms with the same head-to-tail junctions, but different internal exon composition. As observed in this study and other previous reports^{2,5,18,21}, multiple circRNAs with different junctions could form from the same gene loci. The identification of circRNA isoforms with the same junction, but different internal exons, adds another layer to circRNA diversity. The fact that the internal exon composition cannot be simply predicted using junction exons necessitates the experimental determination of full-length sequence of a circRNA before any further functional investigation.

We found that circRNAs were most abundant in brain, consistent with a recent report analyzing circRNAs in fly heads²². Furthermore, the brain-expressed circRNAs were derived from gene loci that also code for proteins enriched for synapse-related functions. To examine whether circRNAs themselves might be associated with the function of synapses, we studied both synaptosomes and the microdissected neuropil from hippocampal slices and found in these samples a relative enrichment of circRNAs compared with their host linear transcripts. In addition, to the best of our knowledge for the first time, we visualized individual circRNA species directly both *in vitro* and *in vivo* (in hippocampal slices). We observed the localization of circRNAs in both the cell body and the dendrites of neurons, similar to what has been observed for both mRNAs⁹ and other regulatory RNAs such as miRNAs²³.

These findings are interesting in light of recent debate in the field concerning the question of circRNA function. Thus far, clear functions have been established for two circRNAs^{4,5}. A recent study suggested that the majority of circRNAs are mere side products of pre-mRNA

splicing¹⁸. Other studies have suggested that circRNAs may have biological functions based on the observation that even lowly expressed circRNAs are regulated²⁴. As conservation in evolution often implies functionality, we analyzed the conservation of mouse circRNA sequences across vertebrates. Compared with splicing sites not involved in circRNA biogenesis, the exonic sequences around the circRNA head-to-tail junctions showed higher conservation (Fig. 2e). Moreover, we analyzed the overlap of circRNAs detected in rat and mouse, and found 23.6% of the circRNAs identified in mouse neuropil were also expressed in rat neuropil (Supplementary Fig. 2e). This observation is consistent with a recent study in which 20% of mouse circRNAs were detected in human cell lines¹⁸, but higher than in another study in which only 4% of the mouse circRNAs were identified in human samples⁵. The difference might be explained by different sampling depths, as most identified circRNAs were expressed at low levels and might therefore 'stochastically' escape detection. Indeed, the circRNAs detected in both mouse and rat samples were clearly of much higher abundance than those detected in only one sample (Supplementary Fig. 2f). This further suggests that circRNAs are conserved, and our observation of a 23% overlap between mouse and rat circRNAs may prove to be an underestimate. Notably, the exonic sequences around head-to-tail junctions detected in both mouse and rat are extremely conserved, strongly suggesting their potential functional relevance (Fig. 2e).

Here we present evidence for the developmental regulation of circRNAs in neurons. There were many circRNAs whose abundance changed independent of the host linear transcript, suggesting a circRNA-specific regulation of biogenesis and/or turnover (Fig. 3c,d). The development of the CNS and brain involves neuronal maturation, neurite outgrowth and synaptogenesis. Non-coding RNAs such as miRNAs and lncRNAs have emerged as important components for regulating these developmental processes^{25,26}. Recently, for example, the lncRNA *RMST* was identified as a factor that is important for neuronal differentiation as well as a co-regulator of *SOX2*, a mediator of neural stem cell fate²⁷. We identified a set of circRNAs that were differentially expressed in the mouse hippocampus at different developmental stages (E18 to P30). A circRNA that was markedly downregulated at later stages arose from the host gene coding for *Rmst*, thereby supporting a potential function of circRNAs in brain development. In contrast, the expression of *circKhlh2* was increased at P30 (P21) compared with E18 (P4), indicating a putative role of this circRNA during synaptogenesis or when mature synapses have formed. In summary, we found a shift in the expression pattern for a large set of circRNAs associated with the onset of synaptogenesis, indicating a role of circRNAs in hippocampal development.

The brain is the most plastic organ and its circuits undergo tight regulation and modification throughout the entire lifespan of animals. Both the stability and flexibility of neuronal networks is central to all behavior, including learning and memory. Experience-dependent alterations in the connectivity of neural networks can result in plasticity of intrinsic excitability and synaptic strength. We induced homeostatic plasticity by treating cultured hippocampal neurons with the GABA_A receptor antagonist bicuculline and observed a dynamic change in circRNA expression. Notably, a circRNA (*circHomer1_a*) derived from the *Homer1* linear transcript was the most significantly upregulated circRNA after plasticity. The *Homer1* protein has a major role in the organization of the postsynaptic density. It is known that neuronal activity causes an increase in expression of an immediate early gene variant of *Homer1*, *Homer1a*, whereas the expression of *Homer1b/c* is relatively unchanged²⁸. The unbalanced regulation of different *Homer1* isoforms contributes to homeostatic downscaling such that the truncated protein encoded by *Homer1a* interferes with the

native interaction between mGluR and Homer1b/c-encoded functional scaffold protein²⁹. The head-to-tail junction formed in *circHomer1_a* uses the splicing donor of intron 5, which is only required to splice the Homer1b/c transcripts, but not the Homer1a transcript. Thus, the biogenesis of *circHomer1_a* could compete with that of *Homer1b/c* mRNA. Upregulation of *circHomer1_a* could then prevent the potential overexpression of Homer1b/c, which would otherwise be detrimental to homeostatic synaptic downscaling. It is therefore conceivable that transcriptional upregulation, the predominant usage of an upstream polyadenylation signal, and circRNA biogenesis work together to achieve the same goal, that is, to reduce the interaction of surface mGluR and scaffold Homer protein. However, it should be noted that only a few circRNAs showed co-regulation with their host genes; more common was the observation that circRNAs exhibited changes independent of the cognate mRNA following plasticity.

Finally, as a heterogeneous group of transcripts, it is very likely that circRNAs affect cellular and neuronal function via a diverse set of mechanisms. The different data sets accumulated in this study should serve as a rich resource for future functional research, where genetic perturbation of specific circRNAs followed by careful phenotypic examination in different *in vitro* and/or *in vivo* neuronal systems will be needed to shed more light on circRNA function in the nervous system and specifically to address their role in learning and memory.

METHODS

Methods and any associated references are available in the [online version of the paper](#).

Note: Any Supplementary Information and Source Data files are available in the online version of the paper.

Accession codes. The sequencing data have been deposited at Gene Expression Omnibus (GEO) under accession number [GSE61991](#).

ACKNOWLEDGMENTS

We thank I. Bartnik, N. Fuerst and A. Staab for the preparation of cultured hippocampal neurons and M. Feldkamp and C. Langnick for their excellent technical assistance on sequencing. We thank C. Schanzenbaecher and J. Langer for generating mass spectrometry data and for the bioinformatic evaluation of circRNA translation. E.M.S. is funded by the Max Planck Society, an Advanced Investigator award from the European Research Council, DFG CRC 902: Molecular Principles of RNA-based Regulation, DFG CRC 1080: Molecular and Cellular Mechanisms of Neural Homeostasis, and the DFG Cluster of Excellence for Macromolecular Complexes, Goethe University. As part of the Berlin Institute for Medical Systems Biology at the MDC, the research group of W.C. is funded by the Federal Ministry for Education and Research (BMBF) and the Senate of Berlin, Germany (BIMSB 0315362A, 0315362C). H.L., T.C. and W.S. are supported by the Chinese Scholarship Council (CSC).

AUTHOR CONTRIBUTIONS

X.Y. and G.T. designed and performed all of the bioinformatic analysis and edited the manuscript. I.V., A.B., T.W., I.E. and G.A. designed, conducted and analyzed the experiments and edited the manuscript, with the help of M.W., C.G., C.Q., T.C., X.W., J.H., H.L. and W.S. S.S. performed and analyzed the electrophysiology experiments. W.C. and E.M.S. conceived and supervised the project, and wrote the manuscript.

COMPETING FINANCIAL INTERESTS

The authors declare no competing financial interests.

Reprints and permissions information is available online at <http://www.nature.com/reprints/index.html>.

- Danan, M., Schwartz, S., Edelheit, S. & Sorek, R. Transcriptome-wide discovery of circular RNAs in Archaea. *Nucleic Acids Res.* **40**, 3131–3142 (2012).
- Salzman, J., Gawad, C., Wang, P.L., Lacayo, N. & Brown, P.O. Circular RNAs are the predominant transcript isoform from hundreds of human genes in diverse cell types. *PLoS ONE* **7**, e30733 (2012).
- Wang, P.L. *et al.* Circular RNA is expressed across the eukaryotic tree of life. *PLoS ONE* **9**, e90859 (2014).
- Hansen, T.B. *et al.* Natural RNA circles function as efficient microRNA sponges. *Nature* **495**, 384–388 (2013).
- Memczak, S. *et al.* Circular RNAs are a large class of animal RNAs with regulatory potency. *Nature* **495**, 333–338 (2013).
- Hentze, M.W. & Preiss, T. Circular RNAs: splicing's enigma variations. *EMBO J.* **32**, 923–925 (2013).
- Jeck, W.R. & Sharpless, N.E. Detecting and characterizing circular RNAs. *Nat. Biotechnol.* **32**, 453–461 (2014).
- Hanus, C. & Schuman, E.M. Proteostasis in complex dendrites. *Nat. Rev. Neurosci.* **14**, 638–648 (2013).
- Cajigas, I.J. *et al.* The local transcriptome in the synaptic neuropil revealed by deep sequencing and high-resolution imaging. *Neuron* **74**, 453–466 (2012).
- Zivraj, K.H. *et al.* Subcellular profiling reveals distinct and developmentally regulated repertoire of growth cone mRNAs. *J. Neurosci.* **30**, 15464–15478 (2010).
- Huntzinger, E. & Izaurralde, E. Gene silencing by microRNAs: contributions of translational repression and mRNA decay. *Nat. Rev. Genet.* **12**, 99–110 (2011).
- Rinn, J.L. & Chang, H.Y. Genome regulation by long noncoding RNAs. *Annu. Rev. Biochem.* **81**, 145–166 (2012).
- Yu, Y. *et al.* A rat RNA-Seq transcriptomic BodyMap across 11 organs and 4 developmental stages. *Nat. Commun.* **5**, 3230 (2014).
- Carlin, R.K., Grab, D.J., Cohen, R.S. & Siekevitz, P. Isolation and characterization of postsynaptic densities from various brain regions: enrichment of different types of postsynaptic densities. *J. Cell Biol.* **86**, 831–845 (1980).
- Dunkley, P.R., Jarvie, P.E. & Robinson, P.J. A rapid Percoll gradient procedure for preparation of synaptosomes. *Nat. Protoc.* **3**, 1718–1728 (2008).
- Squire, L.R. Memory and the hippocampus: a synthesis from findings with rats, monkeys, and humans. *Psychol. Rev.* **99**, 195–231 (1992).
- Brakeman, P.R. *et al.* Homer: a protein that selectively binds metabotropic glutamate receptors. *Nature* **386**, 284–288 (1997).
- Guo, J.U., Agarwal, V., Guo, H. & Bartel, D.P. Expanded identification and characterization of mammalian circular RNAs. *Genome Biol.* **15**, 409 (2014).
- Ingolia, N.T., Brar, G.A., Rouskin, S., McGeachy, A.M. & Weissman, J.S. The ribosome profiling strategy for monitoring translation *in vivo* by deep sequencing of ribosome-protected mRNA fragments. *Nat. Protoc.* **7**, 1534–1550 (2012).
- Turrigiano, G.G., Leslie, K.R., Desai, N.S., Rutherford, L.C. & Nelson, S.B. Activity-dependent scaling of quantal amplitude in neocortical neurons. *Nature* **391**, 892–896 (1998).
- Jeck, W.R. *et al.* Circular RNAs are abundant, conserved, and associated with ALU repeats. *RNA* **19**, 141–157 (2013).
- Westholm, J.O. *et al.* Genome-wide analysis of *Drosophila* circular RNAs reveals their structural and sequence properties and age-dependent neural accumulation. *Cell Reports* **9**, 1966–1980 (2014).
- Tai, H.C. & Schuman, E.M. MicroRNA: microRNAs reach out into dendrites. *Curr. Biol.* **16**, R121–R123 (2006).
- Salzman, J., Chen, R.E., Olsen, M.N., Wang, P.L. & Brown, P.O. Cell type-specific features of circular RNA expression. *PLoS Genet.* **9**, e1003777 (2013).
- Guttman, M. *et al.* lincRNAs act in the circuitry controlling pluripotency and differentiation. *Nature* **477**, 295–300 (2011).
- Mercer, T.R. *et al.* Long noncoding RNAs in neuronal-glial fate specification and oligodendrocyte lineage maturation. *BMC Neurosci.* **11**, 14 (2010).
- Ng, S.Y., Bogu, G.K., Soh, B.S. & Stanton, L.W. The long noncoding RNA RMST interacts with SOX2 to regulate neurogenesis. *Mol. Cell* **51**, 349–359 (2013).
- Bottai, D. *et al.* Synaptic activity-induced conversion of intronic to exonic sequence in Homer 1 immediate early gene expression. *J. Neurosci.* **22**, 167–175 (2002).
- Hu, J.H. *et al.* Homeostatic scaling requires group I mGluR activation mediated by Homer1a. *Neuron* **68**, 1128–1142 (2010).

ONLINE METHODS

Tissue collection and hippocampal microdissections. Wild-type C57B6 or C57BL/6J-Etv1-ARRAy TS88 (male and female) mice and Sprague Dawley (male) rats were housed in standard cages and fed standard lab chow and water *ad libitum*. All animal work was performed following regulations of German animal welfare law. For the developmental studies, hippocampi were dissected from mice at the age of E18, P1, P10 and P30. For tissue profiling, two wild-type C57B6 male mice at the age of 20 weeks were used to dissect the brain, heart, liver, lung and testes. To profile distinct sub-neuronal compartments (somata and neuropil), C57BL/6J-Etv1-ARRAy TS88 male and female mouse and rat male hippocampal slices (500 μ m) were prepared from 4–5-week-old animals and microdissected as described previously for rat⁹. All tissues were collected in RNA later (Ambion) and subsequently lysed in Trizol (Invitrogen) to extract RNA following the manufacturer's instructions.

Preparation of synaptosomes. Synaptosomes were purified from 20 hippocampi of adult mice (4 weeks old) as previously described¹⁵. The hippocampi were homogenized in ice-cold sucrose buffer (320 mM sucrose, 5 mM HEPES, pH 7.4) with a 15-ml Teflon-glass tissue grinder and homogenized with eight even strokes. The homogenate was subjected to three differential centrifugations (1,000 g for 10 min, supernatant was further subjected to centrifugation at 12,000 g for 10 min followed by 13,000 g for 10 min) before applying one gradient centrifugation (3%, 10%, 15% and 23% PercollPlus (GE Healthcare) in sucrose buffer at 31,000 g for 5 min). The latter resulted in separation into five different fractions. The fraction at the interface of the 15% and 23% Percoll contained the most pure synaptosomes, as verified by western blot (enrichment of AMPA receptor subunit, GluR4, substantial depletion of glial fibrillary marker protein GFAP), and was therefore used for all experiments performed in this study.

Polysome profiling. Mouse brains were collected, snap frozen in liquid nitrogen and stored at -80°C . Frozen mouse whole brain was pulverized under liquid nitrogen and the powder lysed in 1 ml of lysis buffer (10 mM HEPES pH 7.4, 150 mM KCl, 10 mM MgCl_2 , 1% NP40 (vol/vol), 0.5 mM DTT, 100 $\mu\text{g ml}^{-1}$ cycloheximide). After lysing the cells by passing them several times through a 26-gauge needle, the nuclei and membrane debris were removed by centrifugation (15,682 g 10 min, at 4°C). The supernatant was layered onto a 10-ml linear sucrose gradient (10–50%, wt/vol, supplemented with 10 mM HEPES pH 7.4, 150 mM KCl, 10 mM MgCl_2 , 0.5 mM DTT, 100 $\mu\text{g ml}^{-1}$ cycloheximide), and centrifuged in a SW41Ti rotor (Beckman) for 120 min at 160,000 g at 4°C . Fractions were collected from Gradient Fractionator (Biocomp) and digested with 200 μg proteinase K in 1% SDS (wt/vol) and for 30 min at 42°C . RNAs were recovered by extraction with an equal volume of acid phenol-chloroform (pH 4.5), followed by ethanol precipitation, then converted to double stranded library using TruSeq Stranded Total RNA Sample Preparation kit (Illumina) and sequenced using Illumina HiSeq2000 platform.

Pharmacological treatments. Rat primary hippocampal neurons were prepared by pooling hippocampi from 10–20 male and female pups and grown in 6-cm petri dishes at a density of 400K. At DIV28, neurons were treated with bicuculline (Tocris, 40 μM) or a water control for 12 h. Subsequently, cells were scraped using Trizol (Invitrogen) followed by RNA extraction. Rat (4 weeks old, male, Sprague Dawley) hippocampal slices (500 μm) were treated with bicuculline (Tocris, 40 μM) or water control for 4 h on filter paper in a recovery chamber. Subsequently, slices were fixed and re-sectioned (30 μm) using a vibratome.

RNA-seq. Ribosomal RNA was depleted from total RNA from different rat and mouse samples using the RiboZero Gold kit (Epicentre Bio-technologies). Poly(A) RNA was enriched using oligo-dT beads (Invitrogen). RNA-seq library was then generated from either rRNA-depleted or poly(A) enriched RNA using Illumina stranded RNA Sample Prep kit according to the manufacturer's instruction, and was subsequently sequenced for 150 nt from single end on an Illumina HiSeq 2000.

TTO estimation. After removing the Illumina sequencing adaptor at 3' end, the reads were aligned to the mouse (mm9) or rat (rn5.0) genome reference sequences using Tophat2, allowing up to six mismatches. Cufflinks (v2.21)³⁰ was then used to estimate the total transcriptional output based on Ensembl gene

annotation for mouse (mm9, version67) or rat (rn5.0, version72). Since most circRNAs are derived from protein coding genes and lincRNAs (Supplementary Table 3), genes annotated as "protein-coding" or "lincRNA" were retained for further analysis. To compare gene expression between two samples, we converted the FPKM (Fragments per kilobase per million) to TPM (Transcripts per million) using the following formula: $\text{TPM} = \text{FPKM} * 1,000,000 / (\text{sum_of_FPKM})^{31}$.

CircRNA identification and quantification. For each sample, the unmapped reads were aligned to the respective genome reference sequences by BWA³² in local mode (with parameters: -mem -k16). Partial alignments of segments within a single read that mapped to (i) regions on the same chromosome and no more than 1Mb away from each other (ii) on the same strand (iii) but in reverse order, were retained as candidates supporting head-to-tail junction. The strength of potential splicing sites supported by these candidate head-to-tail junction reads was then estimated using MaxEntScan³³. The exact junction site was determined by selecting the donor and acceptor sites with the highest splicing strength score. Candidate circRNAs were reported if the head-to-tail junction was supported by at least two reads and the splicing score was greater than or equal to 10.

To estimate the expression of circRNA, we re-aligned all the unmapped reads to the circRNA candidates. As for most of the circRNAs there is no direct evidence for their exact sequence, we filled in the sequence using existing exon annotation. Sequence at the 5' end was concatenated to the 3' end to form circular junctions. Reads that mapped to the junction (with an overhang of at least 6 nt) were counted for each candidate. TPM was calculated for each circRNA candidate, where the effective length was calculated as: (sequencing length – 2 * 6). The analysis pipeline with a detailed description is publicly available at (<https://code.google.com/p/acfs/>).

RNase R treatment and quantitative PCR. Mouse or rat brain DNase1-treated total RNA (1 μg) was incubated for 15 min at 37°C with or without 3 U μg^{-1} of RNaseR (Epicentre Bio-technologies). RNA was subsequently purified by phenol-chloroform extraction. Reverse transcription was performed using random hexamers and reverse transcriptase (SSIII, Invitrogen). Quantitative PCR was done using SYBR green master mix (Roche). For circRNA transcripts, one primer was designed to anneal at the circular junction whereas the other was within the circRNA transcript. For linear transcripts, both primers were designed to amplify the sequence that is not part of any circRNA derived from the same gene locus. All quantitative PCR primers are listed in Supplementary Table 4.

PacBio sequencing of RT-PCR products. The RT-PCR products obtained from mouse brain and rat brain samples, as described in the previous section, were directly sequenced using PacBio RS system as previously described³⁴.

Processing of PacBio sequencing data. Circular consensus reads (CCSreads) obtained from PacBio sequencing were aligned to custom database (consisting of sequences from both linear mRNAs and circRNAs) using Blast (parameters: -evalue 1E-10 -word_size 9). We reported the alignments with identity higher than 95% for both linear and rolling-circle products using an in-house perl script.

Conservation analyses. The positions of rat circRNAs were converted to mouse (mm9) genome coordinates using the UCSC liftOver tool, then were intersected with mouse circRNA using BEDTools. To examine the evolutionary conservation of the sequences around mouse circRNA junctions, we downloaded PhastCons scores for alignment of 29 vertebrate genomes with mouse (mm9) from (<http://hgdownload.soe.ucsc.edu/goldenPath/mm9/phastCons30way/vertebrate/>). To rule out possible biases, we compared the sequences around the splicing sites involved against those not involved in the formation of head-to-tail junction from the same gene locus.

Gene Ontology enrichment analysis. We performed Gene Ontology enrichment analysis using DAVID (<http://david.abcc.ncifcrf.gov>)^{35,36}. The background gene set consists of all expressed genes (TTO > 0.01) and the test gene set consists of all expressed circRNA-hosting genes. In Supplementary Figure 2a, we chose a background gene set consisting of the 1,000, 2,000, 3,000, 5,000, 10,000 most highly expressed genes (top1k, top2k, top3k, top5k, top10k), and then tested for the enrichment of GO terms for the circRNA-hosting genes within the same gene set, respectively.

High-resolution *in situ* hybridization in primary cells and slices. Dissociated rat hippocampal neurons were prepared and maintained as described previously³⁷. 4-week-old rats were perfused with 1× PBS and 4% paraformaldehyde solution (vol/vol), the lung and liver were dissected, sliced to 1 mm, and fixed for 3 h. Lung and liver cells were dissociated and plated to poly-L-lysine-coated dishes as described³⁸. We performed *in situ* hybridization using the QuantiGene ViewRNA miRNA ISH Cell Assay for Fluorescence miRNA and RNA *In situ* Hybridization (RNA FISH) with custom-made probes targeting the circRNA exon junctions or the cognate mRNA (see **Supplementary Table 5** for circRNA probe sequences). Cultured neurons (DIV 26–28 or DIV 4/21 for developmental studies) were fixed for 1 h at 21–23 °C using a 4% paraformaldehyde solution (4% paraformaldehyde, 5.4% glucose (wt/vol), 0.01 M sodium metaperiodate in lysine-phosphate buffer). The *in situ* hybridization was performed following the manufacturer's protocol omitting the dehydration/rehydration step as well as the protease treatment. Dendrites were stained using an anti-Map2 antibody (Millipore AB5622, 1:1,000 dilution). Liver cells were stained with anti-Albumin antibody (Abcam ab106582, 1:50 dilution) and lung cells with anti-Heme Oxygenase 1 antibody (Abcam ab13243, 1:200 dilution). For *in situ* hybridization in hippocampal slices, slices were dissected and fixed overnight in 4% PFA in PBS solution at 4 °C, gently shaking. Hippocampal slices were embedded in 4% low melt agarose and 30-μm sections were prepared using a vibratome (Leica VT 1200S). The *in situ* hybridization was performed as described above with a few modifications from the manufacturer's protocol: the slices were post-fixed for 10–15 min at 21–23 °C, washed with PBS and incubated for 15 min with the detergent solution. After completion of the *in situ* hybridization the slices were blocked for 1 h at 21–23 °C in 1% BSA/1% Triton X-100 in PBS (wt/vol for BSA and vol/vol for Triton X-100). Slices were incubated with the primary antibody anti-Map2 (Millipore AB5622, 1:1,000 dilution) overnight at 4 °C to stain dendrites, washed three times with 1× PBS and incubated with the secondary antibody (Invitrogen, A11008, Alexa 488-goat anti-rabbit; 1:1,000 dilution) and DAPI (1:1,000 dilution) to visualize nuclei for 2 h at 21–23 °C.

Image acquisition and processing. Confocal microscopy was performed using a Zeiss LSM780 confocal laser fluorescence microscope system. Image analysis was done from z stacks of confocal image series of 10–30 confocal planes taken at 35–50-μm intervals using a 40× oil immersion objective. For analysis, conducted in a non-blind manner, cell bodies were circumscribed and dendrites straightened using the software ImageJ. To quantify the *in situ* signal in cell bodies, the average fluorescence intensity was measured per z stack and normalized to the area of the circumscribed cell body. In dendrites the particle abundance was determined using a custom MATLAB script, then the number of particles was normalized to the area of the straightened dendrite. The statistical significance of the *in situ* data was tested using either an unpaired *t*-test or Mann-Whitney *U* test according to the normality of the distribution pre-tested using Lilliefors test.

Electrophysiology. Whole-cell patch-clamp recordings were made with an Axopatch 200B amplifier from cultured hippocampal neurons (DIV 28–29) bathed in HBS containing 119 mM NaCl, 5 mM KCl, 2 mM CaCl₂, 2 mM MgCl₂, 30 mM glucose, 10 mM HEPES [pH 7.4; ~310 mOsm] plus 1 μM TTX and 20 μM bicuculline. Whole-cell pipette internal solution contained 120 mM potassium gluconate, 20 mM KCl, 0.1 mM EGTA, 2 mM MgCl₂, 2 mM ATP, 0.4 mM guanosine triphosphate, 10 mM HEPES (pH 7.2; ~300 mOsm) and the pipette resistances ranged from 4–6 MΩ. Bicuculline was added in conditioned media for 12 h and the media was replaced with the HBS 15 min before recording. Neurons were voltage clamped at –70 mV while the series resistance was left uncompensated during the recordings. mEPSCs were analyzed offline using Stimfit³⁹ software by employing a template-matching algorithm. Recordings were started 5 min after patching and the recording duration usually ranged from 5–10 min. Statistical differences between experimental conditions were determined by Mann-Whitney *U* test.

Potential miRNA binding sites. To quantify miRNA binding sites, exonic sequences within each circRNA were concatenated using Ensembl annotation, and the number of predicted miRNA binding sites (7mer-m8)⁴⁰ for all miRNA (deposited in miRBase version19)⁴¹ was counted. As a control, the same procedure was performed on CDS and 3' UTR of the protein-coding genes.

Potential RBP binding sites. We predicted the RBP binding sites based on their sequencing motifs deposited in RBPDB⁴². Predicted RBP binding sites on circRNAs were compared to those on CDS and 3' UTR of protein-coding genes.

Potential translatability of circRNAs. To estimate the translational capacity of circRNAs, we studied their association with ribosome complexes. We performed polysome profiling on mouse brain and ribosome footprinting on rat brain. Sequencing reads from four fractions of mouse brain (free, 60S, 80S and polysome) and RPFs of rat brain were aligned to circRNAs using BWA, and reads spanning the circular junctions were counted and converted to TPM as described above.

To investigate potential peptides arising from circRNA candidates, a liquid chromatography mass spectrometry sequencing was conducted on total lysate from 21-d-old primary neurons without any pharmacological or electrophysiological treatment. The genomic representation of circRNA candidates was translated in six potential frames (three frames per strand) and the position of the circRNA junction was recorded. This custom database was merged together with the rat protein RefSeq database and was used as a template for peptide matching with Mascot. A custom Perl script was used to identify peptides crossing the circular junction position—such peptides could only arise from circRNA translation.

Statistical analysis. For statistical analysis, two-sided one-sample *t*-test (**Fig. 1f**), two-sided unpaired *t*-test with Welch's correction (**Figs. 2b** and **3c,f**) and two-sided Mann-Whitney *U* test (**Fig. 4a,e**) were performed. In **Figures 1f, 2b** and **3c**, whiskers show extreme data points no more than 1.5 times the interquartile range; and in **Figures 3f** and **4a,e** whiskers show minimum to maximum. The statistical significance of the *in situ* data was tested using either an unpaired *t* test or Mann-Whitney *U* test since the normality of the distribution was pretested using Lilliefors test. No statistical methods were used to predetermine sample sizes, but our sample sizes are similar to those generally employed in the field. Data collection and analysis were not performed blind to the conditions of the experiments and no randomization of data was performed.

A **Supplementary Methods Checklist** is available.

30. Roberts, A., Pimentel, H., Trapnell, C. & Pachter, L. Identification of novel transcripts in annotated genomes using RNA-Seq. *Bioinformatics* **27**, 2325–2329 (2011).
31. Li, B. & Dewey, C.N. RSEM: accurate transcript quantification from RNA-Seq data with or without a reference genome. *BMC Bioinformatics* **12**, 323 (2011).
32. Li, H. & Durbin, R. Fast and accurate short read alignment with Burrows-Wheeler transform. *Bioinformatics* **25**, 1754–1760 (2009).
33. Yeo, G. & Burge, C.B. Maximum entropy modeling of short sequence motifs with applications to RNA splicing signals. *J. Comput. Biol.* **11**, 377–394 (2004).
34. Sun, W. *et al.* Ultra-deep profiling of alternatively spliced *Drosophila* Dscam isoforms by circularization-assisted multi-segment sequencing. *EMBO J.* **32**, 2029–2038 (2013).
35. Huang, D.W., Sherman, B.T. & Lempicki, R.A. Systematic and integrative analysis of large gene lists using DAVID bioinformatics resources. *Nat. Protoc.* **4**, 44–57 (2009).
36. Huang, D.W., Sherman, B.T. & Lempicki, R.A. Bioinformatics enrichment tools: paths toward the comprehensive functional analysis of large gene lists. *Nucleic Acids Res.* **37**, 1–13 (2009).
37. Aakalu, G., Smith, W.B., Nguyen, N., Jiang, C. & Schuman, E.M. Dynamic visualization of local protein synthesis in hippocampal neurons. *Neuron* **30**, 489–502 (2001).
38. Yamashita, K., Kusakabe, M. & Sano, M. A simple and rapid method of dissociating hepatocytes from fixed liver of the mouse. *Stain Technol.* **56**, 29–33 (1981).
39. Schlögl, A., Jonas, P., Schmidt-Hieber, C. & Guzman, S.J. Stimfit: a fast visualization and analysis environment for cellular neurophysiology. *Biomed. Tech. (Berl)* published online, doi:10.1515/bmt-2013-4181 (7 September 2013).
40. Bartel, D.P. MicroRNAs: target recognition and regulatory functions. *Cell* **136**, 215–233 (2009).
41. Griffiths-Jones, S. The microRNA registry. *Nucleic Acids Res.* **32**, D109–D111 (2004).
42. Cook, K.B., Kazan, H., Zuberi, K., Morris, Q. & Hughes, T.R. RBPDB: a database of RNA-binding specificities. *Nucleic Acids Res.* **39**, D301–D308 (2011).